Pressure Distributions and Flow Regimes: An integrated Approach For CO_2 Sequestration Project Design and Evaluation

Introduction

The CO_2 storage capacity of shale reservoirs is exclusively determined by three items. The first is the free gas that is stored in the pore space of shale reservoirs represented by organic and inorganic pore space, and the natural and hydraulic fractures. The free space offered by inorganic matters is often considered non-significant due to the lack of connectivity of the pore space of inorganic matters. Nevertheless, the organic matters provide a significant pore space for storing the CO_2 free gas. The second is the adsorbed gas by the surface of the organic matters and clay minerals. The adsorption mechanisms of clay minerals are more efficient than the organic matters due to their high surface areas and swelling behavior. The adsorbed gas may have the biggest contribution to the CO_2 storage capacity (Wu et al. 2022). The third is the dissolved CO_2 in the kerogen. Kerogen is characterized by the high porosity and specific surface area as well as the high attraction to CO_2 molecules. Therefore, these molecules are easily adsorbed by the kerogen that in turn provides a significant storage capacity to CO_2 (Zhu et al. 2019).

Estimating the storage capacity of shale reservoirs is a keystone for the CO_2 sequestration projects. Currently, there are three techniques for this purpose. The first is the volumetric-based method that can be applied simply to homogenous reservoirs with simple fluid distribution (Chu et al. 2019). Similar to the volumetric method used for calculating the initial oil or gas in place, this technique requires some basic information about the reservoir of interest such as thickness, porosity, drainage area, and saturation. However, applying the volumetric models in shale reservoirs may lead to misleading results. It does not consider the complex structure of these reservoirs as well as the flow mechanisms in the micro-structures.

The second technique for estimating CO_2 storage capacity of shale reservoirs is analysing the production history (Xu et al. 2021). In this technique, a history matching by decline curve analysis is used for calculating the total prove volume that could be an expected candidate for CO_2 storage. It is important to emphasize that the classical decline curve analysis is not recommended. Instead, the history matching techniques of shale reservoirs should be used such as SEPD (Valko and Lee 2010), LGM (Clark et al. 2011), CRM (Pan 2016), Beta derivative (Ilk et al. 2007), and Duong model (Duong 2011). For better estimation of the CO2 storage, the availability of the production data for the whole reservoirs is necessary. Moreover, coupling these models with the probabilistic approach and artificial intelligence tools such as machine learning could give reasonable results (de Holanda et al. 2018).

The third technique is the numerical solutions wherein the CO_2 flow mechanisms and the reservoir characteristics are considered. It considers the hydraulic fracture geometry, natural fractures intensity and connectivity, and organic and inorganic contents. Therefore, it is currently more adopted than the others due to its accuracy in CO_2 storage capacity estimation. However, it requires utilizing powerful industrial simulation tool (Cao et al. 2020).

Pressure distribution and flow regimes

Considering a hydraulically fractured shale reservoir that is shown in Fig. (1). The reservoir of interests is a rectangular shape whose boundaries are $(2x_e, 2y_e)$ and its thickness is (h). Multiple hydraulic fractures are assumed symmetrically propagated in the porous media so that the fracture half-length is (x_F). The reservoir consists of two porous media. The first is the stimulated reservoir volume (SRV) where the hydraulic fractures are propagated. This volume is determined by the porous media between two adjacent fractures and extended from the wellbore to the fracture tips. The second is the unstimulated reservoir volume (USRV) where no hydraulic fracture are existed. This volume is determined by the porous media extended beyond fracture tips to the reservoir boundary.

The analytical model of the wellbore pressure build-up at the point where the hydraulic fractures transect the wellbore is given by:

$$\overline{P_{wD}} = \frac{\pi}{sF_{cD}\sqrt{f_5(s)}\tanh[\sqrt{f_5(s)}]} \quad (1)$$

When CO_2 is injected, the difference between reservoir pressure during injection (P_r) and the depleted pressure before injection (P_d) builds-up. The build-up pressure pulse moves inside the hydraulic fractures at early injection time. Then the pulse moves to the natural fractures of the SRV, the matrix, kerogen, and the organic matters of this volume. At the same time, the pulse transfers to the natural fractures of the USRV and thereafter its matrix, kerogen, and the organic matters.

The maximum pressure build-up is observed close to the horizontal wellbore while the minimum is seen close to the fracture tips. The pressure pulse increases with time as far as the injection of CO_2 is proceeded. At early injection time, this pulse may not reach the fracture tips, however, at some time later, the pulse reaches the tips. Therefore, the time at which the pressure pulse has reached the tips gives an indication that the hydraulic fractures have totally filled by the CO_2. This time is a function of a lot of parameters such as CO_2 injection rate, fracture geometry and conductivity. The injection rate and the fracture conductivity expediates this time. Furthermore, the

higher conductivity is the lower pressure build-up inside hydraulic fractures is. Fig. (1) shows the impact of fracture conductivity.

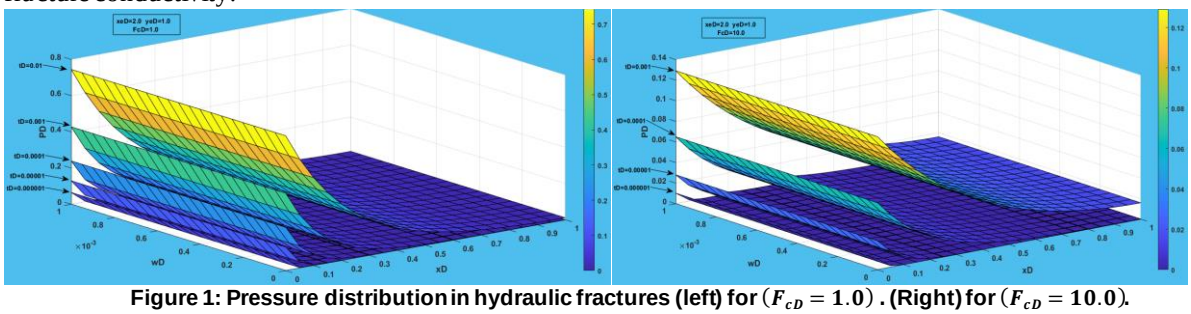

Figure 1: Pressure distribution in hydraulic fractures (left) for $(F_{cD} = 1.0)$. (Right) for $(F_{cD} = 10.0)$.

The pressure pulse moves from hydraulic fractures to the natural fractures of the SRV first and then to the matrix, kerogen, and organic particles sequentially. The distribution of the pressure pulse depends on a lot of parameters such as (η_{fD}). The ratio of the hydraulic diffusivity of hydraulic and natural fractures (η_{fD}) is controlled mainly by the petrophysical properties of the hydraulic and natural fractures such as the permeability. Therefore, the pressure pulse moves very fast when this permeability is high and vice versa. Moreover, the pressure drop inside natural fractures increases when the permeability of these fractures is low. Fig. (2) depicts the pressure distribution for two hydraulics diffusivity ratios $(\eta_{fD} = 100.0)$, and $(\eta_{fD} = 1000.0)$ respectively. Apparently, the maximum pressure drop inside these fractures is seen close to the hydraulic fracture face while the minimum is seen close to the no-flow boundary between two adjacent hydraulic fractures.

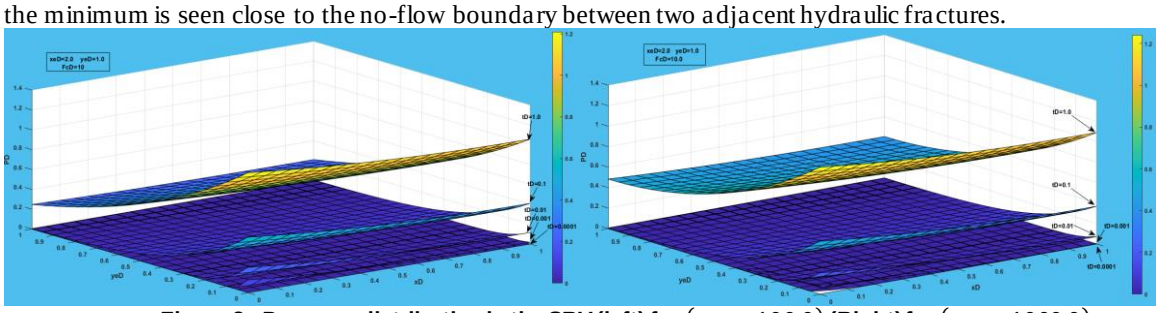

Figure 2: Pressure distribution in the SRV (left) for $(\eta_{fD} = 100.0)$ (Right) for $(\eta_{fD} = 1000.0)$.

The injected CO_2 flows from the natural fractures of the SRV to its matrix. CO_2 spreads inside the matrix that is characterized by ultralow permeability and complex structure. It consists of inorganic matters where clay minerals are imbedded, kerogen particles, and micro-size pores. CO_2 diffuses in the matrix by three flow mechanisms. The first is the adsorption mechanism wherein part of the CO_2 is adsorbed by the surface of clay minerals. The second is the slip flow of the gas to the kerogen particles while the third is the flow in the micropores of the matrix. At the same time, part of the injected CO_2 flows to the natural fractures of the USRV. Because of that, the pressure build-up inside the USRV could take some time to be observed. When the matrix of the SRV is fully saturated by the CO_2, the flow of CO_2 continues from the natural fractures of the SRV to the natural fractures of the USRV. Apparently, the petrophysical properties of the SRV and USRV, mainly the permeability, play the crucial role in this flow. Therefore, as much as the permeability divergence between the natural fractures of the SRV and USRV is small, the CO_2 flows very fast and could reach the reservoir boundary (x_{eD}, y_{eD}) in a short time and vice versa. Fig. (3) demonstrates the pressure distribution in the USRV for $(\eta_{rD} = 0.1)$, and $(\eta_{rD} = 0.001)$ respectively.

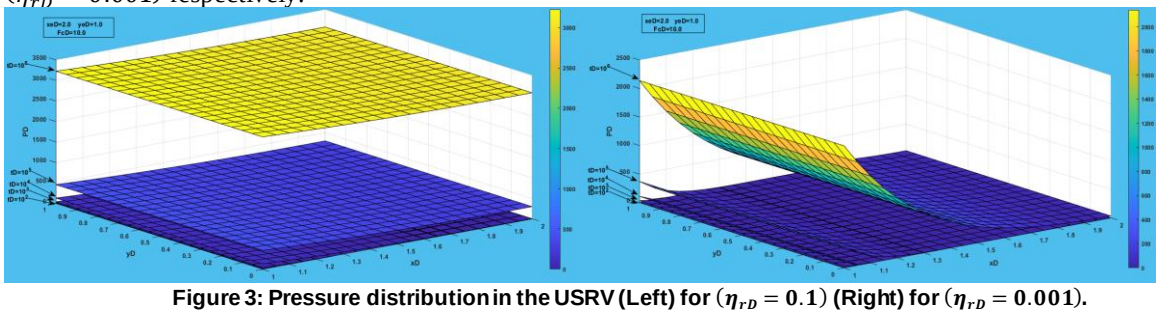

Figure 3: Pressure distribution in the USRV (Left) for $(\eta_{rD} = 0.1)$ (Right) for $(\eta_{rD} = 0.001)$.

1- Hydraulic fracture linear flow regime

This flow regimes develops at early injection time when CO_2 flows linearly inside hydraulic fractures. It is controlled by the hydraulic fracture conductivity and characterized by a straight line of a slope of $(1/2)$ on the log-log plot of the pressure derivative. Fig. (4 Left) depicts the pressure build-up and its derivative behaviors with the injection time for three hydraulic fracture conductivities $(F_{cD} = 1.0, 10, 20)$. This figure is designed for the calculated pressure build-up inside the wellbore i.e., $(x_D = x_{wD})$ where the wellbore intersects the fractures, while

the pressure distribution along the hydraulic fractures is shown in Fig. (4 Right) for a specific fracture conductivity $(F_{cD} = 10)$. Fig. (4 Left) tells us that CO_2 pressure could build-up very slow when the fracture conductivity is high, thus, the pressure build-up pulse could take a long time to reach the fracture tips. While Fig. (4 Right) says that the pressure build-up inside hydraulic fractures sharply declines toward the fracture tips. It is important to emphasize that the CO_2 flow inside hydraulic fractures is better described by the non-Darcy flow rather than the Darcy flow. The injection time of CO_2 during hydraulic fracture linear flow regime, in field units, is calculated from the dimensionless time at which the pressure pulse has reached the fracture tips. This time is given by:

$$(t_{inj})_{hf} = \frac{(\phi\mu c_t)_{srv} x_f^2}{0.000263 k_{srv}} (t_D)_{hf} \quad (2)$$

therefore, CO_2 geosequestration capacity (CGC) of a single hydraulic fracture can be determined by:

$$(CGC)_{hf} = \frac{(\phi\mu c_t)_{srv} x_f^2}{0.000263 k_{srv}} (t_D)_{hf} (\varphi Q_{sc}) \quad (3)$$

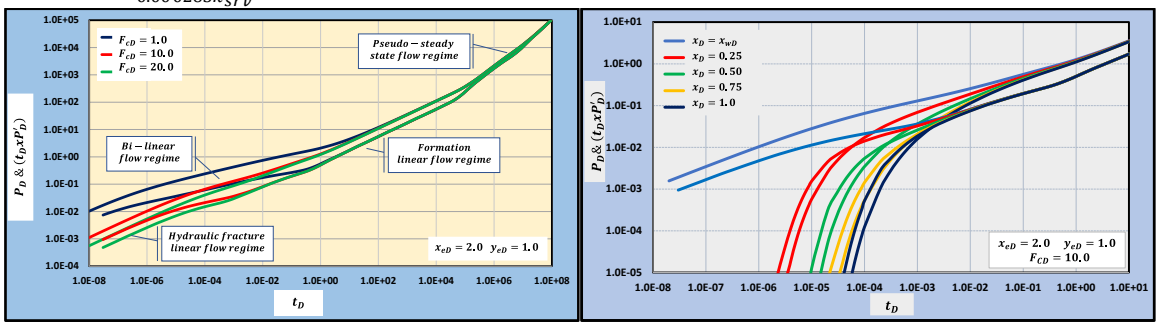

Figure 4: Pressure build-up and its derivative behavior calculated at (Left) ($(x_D = x_{wD})$ (Right) $(x_{wD} \le x_D \le 1.0)$.

2- Bi- linear flow regime

This flow regime develops when the CO_2 flows inside the natural fractures of the SRV. It is typically observed after the hydraulic fracture linear flow regime and characterized by a straight line of a slope of $(1/4)$ on the log-log plot of the pressure derivative as it is shown in Fig. (4 Left). This flow regime is mainly controlled by the characteristics of the natural fractures and the matrix of the SRV as well as the characteristics of the hydraulic fractures, and the natural fractures and matrix of the USRV. The injected CO_2 spreads inside the matrix after leaving the natural fractures. CO_2 diffuses in the matrix by three flow mechanisms. The first is the adsorption mechanism wherein part of the CO_2 is adsorbed by the surface of clay minerals. The second is the slip flow of the gas to the kerogen particles while the third is the flow in the micropores of the matrix. The injection time of CO_2 during hydraulic fracture linear flow regime, in field units, is calculated from the dimensionless time at which the pressure pulse has reached the no-flow boundary between two adjacent hydraulic fractures i.e., $(y_D = y_{eD})$.

$$(t_{inj})_{bf} = \frac{(\phi\mu c_t)_{srv} x_f^2}{0.000263 k_{srv}} (t_D)_{bf} \quad (4)$$

where $(t_D)_{bf}$ is the difference between the start and end time of the bi-linear flow regime. Therefore, CO_2 geosequestration capacity (CGC) of the SRV is determined by:

$$(CGC)_{bf} = \frac{(\phi\mu c_t)_{srv} x_f^2}{0.000263 k_{srv}} (t_D)_{bf} (\varphi Q_{sc}) \quad (5)$$

3- Formation linear flow regime

This flow regimes develops when the CO_2 flows from the natural fractures of the SRV to the natural fractures of USRV. It is characterized by a straight line of slope $(1/2)$ on the log-log plot of the pressure derivative as it is demonstrated in Fig. (4 Left). From the natural fracture, CO_2 diffuses to the matrix of the USRV and later to the kerogen particles and organic contents. It is controlled by the characteristics of the natural fractures and matrix of the USRV. Two flow mechanisms occurs when the CO2 diffuses throughout the matrix. The first is the dissolution of the CO_2 in the organic matters energized by the similar characteristics of CO_2 molecules and the organic matters. The second is the diffusion flow mechanism that takes place when the dissolved gas, driven by the concentration difference, diffuses easily in the organic matter. While the flow inside the natural fractures can be described by the Darcy flow. The injection time of CO_2 during formation linear flow regime, in field units, is calculated from the dimensionless time at which the pressure pulse has reached the reservoir boundaries i.e., $(x_D = x_{eD})$. This time is given by:

$$(t_{inj})_{ff} = \frac{(\phi\mu c_t)_{srv} x_f^2}{0.000263 k_{srv}} (t_D)_{ff} \quad (6)$$

where $(t_D)_{ff}$ is the difference between the start and end time of the formation linear flow regime. Therefore, CO_2 geosequestration capacity (CGC) of the USRV is determined by:

$$(CGC)_{ff} = \frac{(\phi\mu c_t)_{srv} x_f^2}{0.000263 k_{srv}} (t_D)_{ff} Q_{sc} \quad (7)$$

4- Pseudo-steady state flow regime

This flow regime represents the impact of the reservoir boundaries on the CO_2 pressure build-up during injection. It is observed when the reservoir boundaries have been approached by the pressure pulse. It is characterized by a straight line of a unit slope for the pressure and pressure derivative curves on the log-log plot vs production time. This flow regime is mainly controlled by the reservoir configuration or the drainage area (x_{eD}, y_{eD}). Because of the matrix ultralow permeability, the reservoir boundaries may need for a long time to be reached, therefore, the pseudo-steady state flow regime is typically seen at very late injection time. The corresponding time to the initial reservoir pressure or the constraint pressure can be calculated and used to calculate the geosequestration capacity (CGC) of the reservoir:

$$(CGC)_r = \frac{(\phi\mu c_t)_{srv} x_f^2}{0.000263 k_{srv}} (t_D)_r Q_{sc} \quad (8)$$

$$(t_{inj})_r = \frac{(\phi\mu c_t)_{srv} x_f^2}{0.000263 k_{srv}} (t_D)_r \quad (9)$$

where $(t_D)_r$ is the correspondent time, in dimensionless form, to the initial reservoir pressured or the constraint pressure.

Conclusions

The study has reached several conclusions. The characteristics of the organic matter, kerogen, and the micro-size scale matrix do not significantly impact the pressure distribution and flow regimes. Conversely, the pressure distribution and flow regimes are significantly impacted by the characteristics of the hydraulic and natural fractures. The hydraulic fractures may offer a reasonable capacity for CO_2 storage, meanwhile the capacity of stimulated and unstimulated reservoir volume is controlled by reservoir configuration and fracture spacing. The constrained pressure may strictly reduce the total capacity of CO_2 storage in the reservoir. The total volume of the injected CO_2 can be determined from the pressure point when the injection pulse has reached to reservoir boundary. Beyond this point, it is not recommended to inject CO_2 as it could increase reservoir pressure more than initial pressure. The pressure of depleted reservoir before injection is a key parameter in the design and evaluation of the CO_2 storage in shale reservoirs.

References

Cao, Cheng et al. 2020. Utilization of CO_2 as Cushion Gas for Depleted Gas Reservoir Transformed Gas Storage Reservoir. Energies, 13(3). https://doi.org/10.3390/en13030576

Chu, H. et al. 2019. Estimating carbon geosequestration capacity in shales based on multiple fractured horizontal well: A case study. Journal of petroleum science and engineering (Geoenergy Science and engineering), 181. https://doi.org/10.1016/j.petrol.2019.06.043

Clark, A. J., Lake, L. W., and T. W. Patzek, 2011. Production Forecasting with Logistic Growth Models. Paper presented at the SPE Annual Technical Conference and Exhibition, Denver, Colorado, USA, October 2011. https://doi.org/10.2118/144790-MS

de Holanda, Rafael Wanderley, Gildin, Eduardo, and Peter P. Valkó., 2018. Combining Physics, Statistics, and Heuristics in the Decline-Curve Analysis of Large Data Sets In Unconventional Reservoirs. SPE Reservoir Evaluation & Engineering 21 (03). https://doi.org/10.2118/185589-PA

Duong, Anh N., 2011. Rate-Decline Analysis for Fracture-Dominated Shale Reservoirs. SPE Reservoir Evaluation & Engineering 14 (03): 377–387. https://doi.org/10.2118/137748-PA

Ilk, D., Hosseinpour-Zonoozi, N., Amini, S., and T. A. Blasingame, 2007. Application of the ß-Integral Derivative Function to Production Analysis. Paper presented at the Rocky Mountain Oil & Gas Technology Symposium, Denver, Colorado, U.S.A., April 2007. https://doi.org/10.2118/107967-MS

Pan Zhong, 2016. Revised productivity index equation to improve transient history match for the capacitance resistant model. Thesis submitted to the university of Texas - Austin, USA.

Valkó, Peter P., and W. John Lee, 2010. A Better Way to Forecast Production from Unconventional Gas Wells. Paper presented at the SPE Annual Technical Conference and Exhibition, Florence, Italy, September 2010. https://doi.org/10.2118/134231-MS

Wu J. et al. 2022. Molecular investigation on CO_2-CH_4 displacement and kerogen deformation in enhanced shale gas recovery. Fuel, 315. https://doi.org/10.1016/j.fuel.2022.12320

Xu et al. 2021. Revisiting field estimates for carbon dioxide storage in depleted shale gas reservoirs: The role of geomechanics. International Journal of Greenhouse Gas Control 105 (2021) 103222. https://doi.org/10.1016/j.ijggc.2020.103222

Zhu et al. 2019. Adsorption and dissolution behaviors of CO_2 and n-alkane mixtures in shale: Effects of the alkane type, shale properties and temperature. Fuel, 253.https://doi.org/10.1016/j.fuel.2019.05.00